J Mater Sci (2008) 43:5495–5503
DOI 10.1007/s10853-008-2834-4

XPS study of the initial oxidation of the bulk metallic glass $Zr_{46.75}Ti_{8.25}Cu_{7.5}Ni_{10}Be_{27.5}$

S. K. Sharma · T. Strunskus · H. Ladebusch · V. Zaporojtchenko · F. Faupel

Received: 12 June 2007 / Accepted: 25 June 2008 / Published online: 15 July 2008

Abstract The surface oxidation behaviour of the bulk metallic glass $Zr_{46.75}Ti_{8.25}Cu_{7.5}Ni_{10}Be_{27.5}$ was investigated in situ by using X-ray photoelectron spectroscopy (XPS). The initial stages of oxidation at room temperature were studied by exposing the clean alloy specimen surface to varying doses of pure oxygen (up to 1,000 L) in an UHV chamber. Progressive oxidation of Zr, Be and Ti was observed with increasing doses, the major species in the oxide layer being Zr(IV) and Be(II) possibly existing as ZrO_2, BeO, while Cu and Ni remained in their elemental forms. High temperature in situ oxidation in the temperature range 423–653 K for a fixed oxygen dose of 300 L was also investigated. Oxidation of Be was observed at all temperatures, while a sharp decrease in the oxidation of Zr and Ti was observed for temperatures at 573 K and above. The results show a preferential oxidation of Be and Zr at room temperature, while at higher temperatures oxidation is controlled by the reduction of oxides of Zr and Ti and the diffusion of oxygen into the alloy bulk. The role of the dissolved carbon impurity in the reduction of the oxides is discussed.

S. K. Sharma (✉) · T. Strunskus · H. Ladebusch · V. Zaporojtchenko · F. Faupel
Lehrstuhl fur Materialverbunde, Technische Fakultät der CAU Kiel, Kaiserstr. 2, 24143 Kiel, Germany
e-mail: sksh@datainfosys.net

S. K. Sharma
Department of Physics, Malaviya National Institute of Technology, J. L. N. Marg, Jaipur 302 017, India

T. Strunskus
Lehrstuhl für Physikalische Chemie 1, Ruhr-Universität Bochum, Universitätstr. 150, 44780 Bochum, Germany

Introduction

Zr-based multicomponent bulk amorphous alloys, e.g. alloys belonging to the family Zr–Ti–Ni–Cu–Be like $Zr_{46.75}Ti_{8.25}Cu_{7.5}Ni_{10}Be_{27.5}$ known as Vitreloy 4 or V4, exhibit a high resistance with respect to crystallization in their supercooled liquid region and at the glass transition. These alloys have a wide supercooled liquid region and are processable in the bulk form at much reduced cooling rates, typically 1–100 K/s unlike very high cooling rates of 10^5–10^6 K/s required for conventional metallic amorphous alloys [1, 2].

Amorphous alloys, in general, are interesting materials both for basic and applied research as they possess a number of attractive properties like high mechanical strength, good ductility, low temperature dependence of resistivity and superior oxidation and corrosion properties. These have basically been attributed to the absence of crystal-like defects in these materials and to their chemical homogeneity [3].

Oxidation studies on these bulk amorphous alloys are important as the alloying elements, especially Zr, Ti and Be possess high reactivity to oxygen. Characterization of surface oxide layers by surface sensitive techniques like X-ray photoelectron spectroscopy (XPS) provides important information about the chemical states of the various alloying elements and their role in oxide film formation. Further, it has been shown that conventional Zr-based amorphous alloys are promising precursors of oxide-supported catalysts [4, 5]. Moreover, knowledge of oxidation behaviour of these alloys is important for their possible applications [6] in oxidizing environments. These were some of the motivating factors for carrying out the present study on this bulk amorphous alloy.

Several investigations on oxidation of conventional metallic glasses are available in the literature [e.g. 7–11]. On the other hand only few investigations on the oxidation

behaviour of bulk metallic glasses have so far been reported in the literature [12–26]. The latest work on oxidation of amorphous alloys pertains to the oxidation of Zr-based bulk amorphous alloys [20–26]. However, in contrast to investigations on long time oxidation of these alloys [8, 9, 12–18, 20–26] only few investigations pertaining to initial oxidation [7, 10, 11, 19] have been reported in the literature. Schneider et al. [12] and Sun et al. [13] observed the preferential oxidation of Zr and Al during the high-temperature oxidation of amorphous $Zr_{60}Al_{15}Ni_{25}$ in dry oxygen. Kiene et al. [14] observed the enhancement of Be at the outermost surface followed by a Be, Zr and Ti rich phase during oxidation of $Zr_{46.75}Ti_{8.25}Cu_{7.5}Ni_{10}Be_{27.5}$ at 573 K in air. Triwikantoro [15] and Köster and Triwikantoro [16] studied the oxidation of several bulk Zr–Cu–Ni–Al bulk glasses in air at 633 K. They found ZrO_2 as the major species with oxidation kinetics being controlled by oxygen diffusion in the scale towards the oxide/glass interface. Dhawan et al. [17, 18] investigated the oxidation of amorphous $Zr_{65}Cu_{17.5}Ni_{10}Al_{7.5}$ in air in the temperature range 591–684 K using thermogravimetric analysis suggesting a parabolic rate law for oxidation of the amorphous phase. In another recent study by Dhawan et al. [23] the analysis of air-formed oxide films on amorphous $Zr_{65}Cu_{17.5}Ni_{10}Al_{7.5}$ in the temperature range 573–663 K by XPS provided support to the previously proposed [18] oxidation mechanisms for this alloy by the same authors. All the reported oxidation studies pertain to direct oxidation in air or oxygen, and to the best of our knowledge an investigation on in situ high-temperature oxidation of a Zr-based bulk metallic glass is still missing in the literature. Such an investigation is desirable to understand the oxidation mechanism of this glass at high temperatures. This was an additional motivating factor to carry out the present study. In a previous study by the present authors [19] a part of the data pertaining to the room temperature native oxidation of $Zr_{65}Cu_{17.5}Ni_{10}Al_{7.5}$ and $Zr_{46.75}Ti_{8.25}Cu_{7.5}Ni_{10}Be_{27.5}$ were reported suggesting ZrO_2 as the major oxidation species.

The present work pertains to the study of the initial oxidation of the bulk amorphous alloy $Zr_{46.75}Ti_{8.25}Cu_{7.5}Ni_{10}Be_{27.5}$ by in situ exposing the clean alloy surface to various doses of pure oxygen (up to 1,000 L) in an UHV chamber at room and high temperatures. The growth of the oxide film was studied using XPS. The high-temperature oxidation for a fixed oxygen dose of 300 L was investigated in the temperature range 423–653 K.

Experimental

Polished specimens (10-mm diameter × 1-mm thickness) of the bulk amorphous alloy $Zr_{46.75}Ti_{8.25}Cu_{7.5}Ni_{10}Be_{27.5}$ were used in these investigations. The alloy displayed a crystallization temperature of 741 K at a heating rate of 20 K/min in a differential scanning calorimeter. The sample preparation details are given elsewhere [27]. Prior to oxidation, the specimen surface was cleaned by argon ion (Ar^+) bombardment with 3 keV energy in the analysis chamber of the electron spectrometer (VG Escalab MKII) until oxygen and carbon signals were reduced to their minimum and very insignificant levels. The ion beam was incident at an angle of 56° to the sample surface normal and the typical ion current was 10 μA. The cleaned specimen surface was exposed to varying doses of pure oxygen (99.998% purity) up to 1,000 L (1 Langmuir unit = 1.33×10^{-6} mbar s^{-1}). For every fresh exposure, the specimen surface was thoroughly cleaned by Ar^+ ion sputtering. For high-temperature oxidation in the temperature range 423–653 K, the cleaned specimen was brought to the preparation chamber (base pressure better than 1×10^{-10} mbar), heated to the desired temperature using resistive heating and exposed to a pure oxygen dose of 300 L. It was ensured using the reported time–temperature–transformation diagram for this alloy [28, 29] that the alloy remained in the amorphous state after annealing at higher temperatures.

The XPS measurements on oxidized specimens were performed using a hemispherical electron analyser (VG MKII) and an unmonochromatized Al K_α X-ray source (energy $h\nu = 1{,}486.6$ eV) operated at 500 W. The base pressure in the analysis chamber was better than 1×10^{-10} mbar during the XPS analysis. The XPS spectra were recorded at a pass energy of 20 eV with an energy resolution of 1.2 eV measured at Ag $3d_{5/2}$ line. Binding energy calibration was checked by the Au $4f_{7/2}$ line of a pure gold foil which appeared at 84.0 eV. A Shirley-type background was subtracted from all spectra prior to processing of the data. Binding energies and relative intensities have been determined using commercially available peak fitting routines (Peakfit 2.0, Jandel). The procedure was as follows: we always started with the spectra obtained from the clean alloy surface. To account for the asymmetric lineshape of the core level lines of metals, we used Asymmetric Double Sigmaoidal peaks and left all parameters free to obtain the best fit. To fit the spectra of oxygen-exposed samples, we kept the lineshape of the metal lines fixed and introduced one or more Gaussians to fit the peaks of the oxides. This procedure gave consistent results for all core level spectra.

Results

Room temperature oxidation

Already before exposure of the sample to oxygen a very weak oxygen peak is noticed in the O 1s spectrum of the

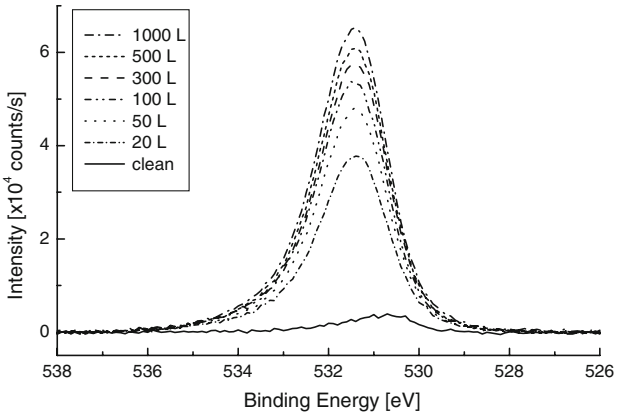

Fig. 1 O 1s XPS spectra for different oxygen exposures for room temperature oxidation. The exposure doses are mentioned in the inset on the figure

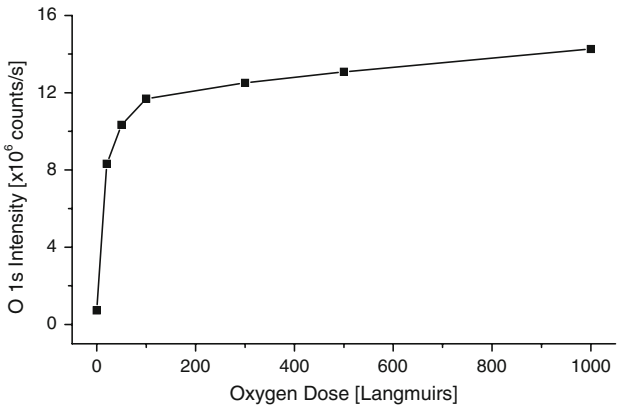

Fig. 2 Oxygen uptake curve showing the plot of measured O 1s intensity against the oxygen dose in Langmuir units (1 L = 1.33×10^{-6} mbar s^{-1}) at room temperature

clean surface (see Fig. 1). This oxygen possibly arises due to the presence of some inherent-dissolved oxygen in the alloy and its segregation to the alloy surface during the sputter cleaning process may not be ruled out. However, it was not possible to carry out a cyclic heating and sputter cleaning procedure to totally get rid of such dissolved impurities due to the possibility of induced crystallization in the amorphous alloy. On exposure to oxygen a strong O 1s peak appears at 531.4 eV, which grows in intensity with increasing exposures. The peak position for O 1s peak is at a somewhat higher binding energy than that normally observed for metal oxides [30]. But in the case of oxidation of Zr and Zr-based alloys the O 1s peak has been reported to appear at relatively higher binding energies [31, 32]. Nishino et al. [31] carried out initial oxidation studies on pure Zr and Zircaloy-2 at room temperature and reported an O 1s peak for ZrO_2 at 531.0 eV, while Kaufman et al. [32] in a similar study on pure Zr reported O 1s peak to occur at 531.4 eV. Therefore, the observation of O 1s peak at 531.4 eV in conjunction with Zr 3d XPS peak (shown in Fig. 3 and discussed below) in our study is consistent with the formation of ZrO_2 on the surface.

The uptake of oxygen on the alloy specimen surface at room temperature is shown in Fig. 2, where the XPS O 1s intensity is plotted as a function of oxygen exposure. It is observed from this figure that at first there is a steep increase up to an exposure of about 100 L. For higher exposures the rate of increase is very small. This change corresponds to the transition from chemisorption and growth of the initial oxide layer on the clean surface to the logarithmic growth phase of the oxide scale, which is controlled primarily by bulk kinetics processes. In the following sections, the changes observed for each element in the alloy are summarized.

The XPS core level spectra of the Zr 3d region for different oxygen exposures are shown in Fig. 3. The Zr

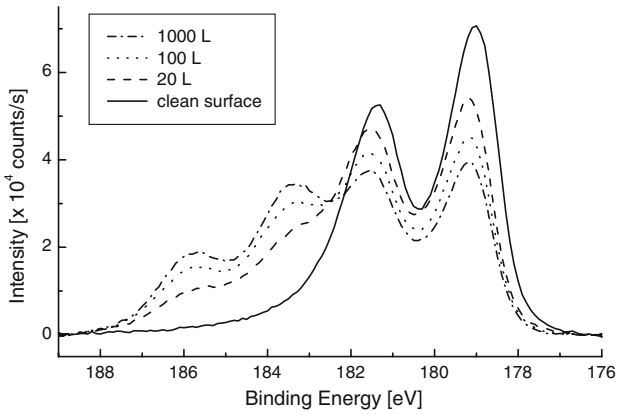

Fig. 3 Zr 3d XPS spectra for different oxygen exposures for room temperature oxidation. The exposure doses are mentioned in the inset on the figure

$3d_{5/2}$ XPS peak on the clean specimen appears at 179.0 eV corresponding to metallic Zr. It should be noted that the clean surface was obtained by prolonged sputter cleaning by Ar^+ ions and in view of the preferential sputtering effects surface composition may be somewhat different from the real bulk composition of the alloy [33]. However, no attempt has been made here to decipher any compositional changes due to these preferential sputtering effects. After oxygen exposure a small shift of 0.2 eV to higher binding energy is observed for all metal core level lines. It may arise as metallic species coexist with the oxide species near the oxide–alloy interface. Upon exposure to oxygen a clear Zr $3d_{5/2}$ oxide peak at 183.4 eV starts building up and grows in intensity with increasing exposures. In the case of initial oxidation of amorphous Zr–Ni alloys the Zr $3d_{5/2}$ peak has been shown to occur at 183.7 eV for ZrO_2 and at 179.0 eV for metallic Zr [10]. In another investigation Satoh et al. [34] have reported the Zr $3d_{5/2}$ peak for ZrO_2 to occur at 183.4 eV. On the other hand Nishino et al. [31]

have reported the Zr $3d_{5/2}$ peak to appear at 182.9 eV for ZrO_2 formation during the initial oxidation of Zircaloy-2. It appears that slight differences in Zr $3d_{5/2}$ position might arise due to the alloying behaviour. Therefore, the peak at 183.4 eV is suggestive of the formation of ZrO_2, perhaps accompanied by a small amount of suboxides. In this connection it is worth mentioning here that Nishino et al. [31] in their investigation on the initial oxidation of Zr and Zircaloy-2 at room temperature observed lower valent suboxides of Zr only at very low oxygen doses (below 5 L) and oxidation at higher doses was dominated by the formation of ZrO_2. The surface of the native oxide shows the Zr $3d_{5/2}$ peak at 183.5 eV. The increase in the zirconium oxide intensity (data not shown) follows the same trend as the increase in the O 1s intensity plotted in Fig. 2. Therefore the oxidation of zirconium seems to be proportional to the total oxygen uptake.

The XPS peak of Be 1s that appears at 111.8 eV on the clean alloy surface shows an oxide component at 114.3 eV (cf. Fig. 4) corresponding to the presence of a Be(II) species possibly in the form of BeO [30] on exposure to pure oxygen. The metallic peak shows some overlap with the Ni 3s peak which appears at 111.0 eV [30]. However, the oxide peak at 114.3 eV has no overlap and information about Be oxidation can be unambiguously obtained from this peak. It is seen from Fig. 4 that the intensity of the oxide peak in Be 1s spectra grows progressively with increasing doses of oxygen with a consequent decrease in the metallic component peak.

The oxide contribution in the Ti 2p XPS spectra (cf. Fig. 5) appears to be not so developed as in the Zr 3d spectra as shown earlier in Fig. 2 suggesting a lower degree of oxidation in the case of Ti. The Ti $2p_{3/2}$ peak appears at 454.2 eV for the clean surface and shifts to 454.5 eV on exposure to pure oxygen with a clear asymmetry on the higher binding energy side (Fig. 5). At higher exposures a small hump at 457.8 eV can be noticed. For the formation of TiO and TiO_2, the Ti $2p_{3/2}$ peak has been reported to appear at 455.0 and 458.8 eV, respectively [30]. It could thus be inferred from Fig. 5 that oxidation of Ti corresponds to the formation of several oxidation states containing Ti(II), Ti(III) and possibly Ti(IV) also. It is thus obvious from Figs. 3–5 that with increasing exposures the metallic component always shows a clear decrease with a consequent increase in the oxide component in the respective figures suggesting that these oxides (consisting of Zr(IV), Be(II) and Ti(II)–Ti(IV)) coexist in the initial oxide film.

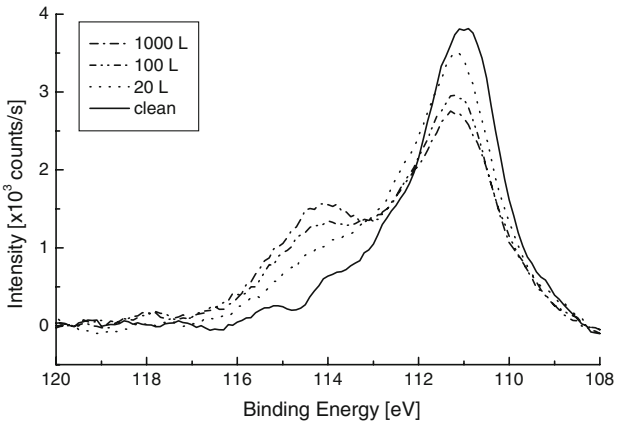

Fig. 4 Be 1s XPS spectra for different oxygen exposures for room temperature oxidation. The exposure doses are mentioned in the inset on the figure

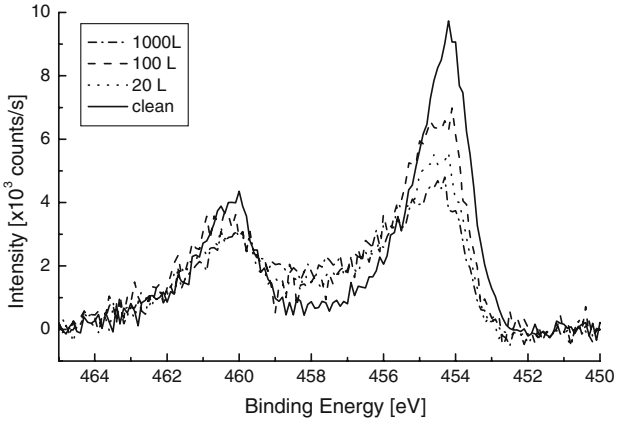

Fig. 5 Ti 2p XPS spectra for different oxygen exposures for room temperature oxidation. The exposure doses are mentioned in the inset on the figure

We note that a C 1s peak (data not shown) was always observed at 282.4 eV on the specimen corresponding to the presence of a small amount of carbon in carbide form. It was practically constant during various exposures with oxygen. This surface carbon may arise due to the segregation of dissolved carbon from the bulk to the surface while the sample was sputter cleaned with energetic (3.0 keV) Ar^+ ions for a long period. Carbide formation can occur with Zr and Ti because of their strong affinity for this process suggesting that very small amounts of Zr and Ti are contained in the carbide form as well.

No oxidation of Cu and Ni on the surface with exposure to oxygen is noticed as the Cu $2p_{3/2}$ and Ni $2p_{3/2}$ XPS peaks remain at the same positions, viz. 933.2 and 853.3 eV, respectively, as for the clean alloy surface. A shift of 0.5 eV in $Ni2p_{3/2}$ with respect to the reported $Ni2p_{3/2}$ peak position (852.8 eV) for the Ni^0 [30] may possibly be attributed for alloying. A similar higher position in Ni $2p_{3/2}$ XPS peak for metallic Ni^0 has also been reported in amorphous Zr–Ni alloys [10, 11]. The Cu $2p_{3/2}$ and Ni $2p_{3/2}$ peaks show a progressive and similar decrease in intensity with progressive oxidation (see Fig. 6). The intensity decrease may arise as the photoelectrons corresponding to these peaks get more and more attenuated by the growing

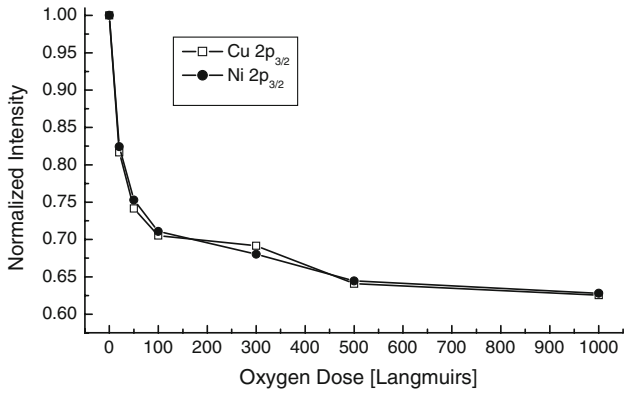

Fig. 6 Development of the normalized Cu $2p_{3/2}$ and Ni $2p_{3/2}$ XPS intensity for room temperature oxidation. The intensities were normalized to Zr 3d intensity to exclude intensity variations between different XPS measurements and the initial intensity of the clean specimen was set to unity

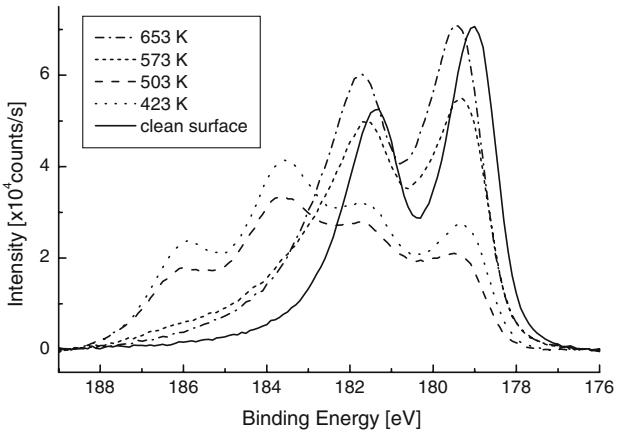

Fig. 7 Zr 3d XPS spectra for in situ oxidation at higher temperatures for a fixed oxygen dose of 300 L. The temperature for each curve is mentioned in the inset on the figure

oxide overlayer. This would suggest that these elements are located at/near the oxide–alloy interface.

Oxidation at higher temperatures

Oxidation of the alloy specimens for a fixed oxygen dose of 300 L was also carried out at higher temperatures in the temperature range 423–653 K. The XPS spectra for Zr 3d, Ti 2p and Be 1s peaks are shown in Figs. 7–9, respectively. From these figures, it is observed that the oxide components of Zr and Ti are drastically reduced at 573 and 653 K and only the oxide component of Be is found at these temperatures. On the contrary, oxide peaks of all the three elements, namely Zr, Ti and Be, are seen during oxidation at lower temperatures, viz. 423 and 503 K. For all the exposures, the O 1s peak (data not shown) remains at 531.6 eV as for the room temperature oxidation. Therefore, only its intensity variation is shown in Fig. 10. Oxide peak

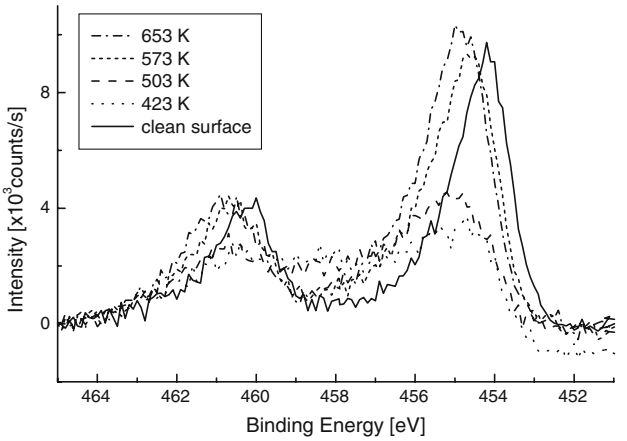

Fig. 8 Ti 2p XPS spectra for in situ oxidation at higher temperatures for a fixed oxygen dose of 300 L. The temperature for each curve is mentioned in the inset on the figure

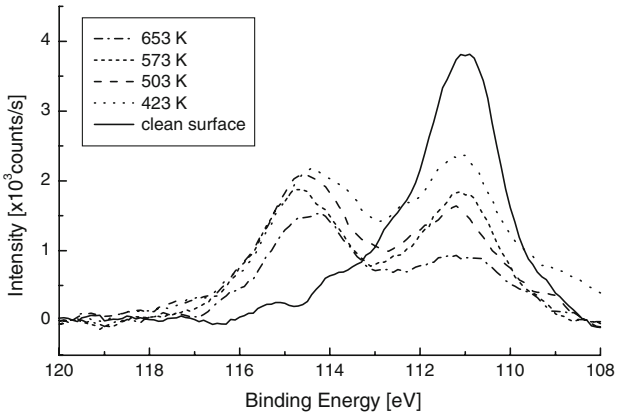

Fig. 9 Be 1s XPS spectra for in situ oxidation at higher temperatures for a fixed oxygen dose of 300 L. The temperature for each curve is mentioned in the inset on the figure

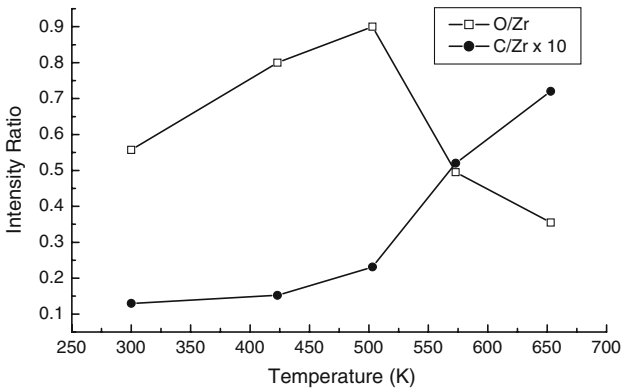

Fig. 10 XPS intensity ratios for (O/Zr) and (C/Zr) versus temperature for in situ oxidation at higher temperatures for a fixed oxygen dose of 300 L

positions for Be, Zr and Ti are the same as observed during initial oxidation at room temperature (see section "Results: Room temperature oxidation") and are suggestive of the

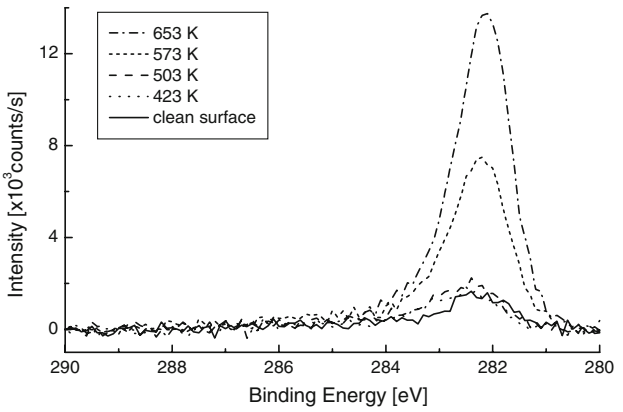

Fig. 11 C 1s XPS spectra for in situ oxidation at higher temperatures for a fixed oxygen dose of 300 L. The temperature for each curve is mentioned in the inset on the figure

presence of Be(II), Zr(IV) and Ti(II)–Ti(IV) species, possibly in the form BeO, ZrO_2 and substochiometric Ti(IV) oxides, respectively. At low oxidation temperatures (423 and 503 K) all three elements are oxidized, whereas this is clearly not the case at elevated temperatures (573 and 653 K). At 573 K and above no stable oxides of Zr and Ti remain on the surface. Interestingly, the oxygen intensity is also drastically reduced at these higher temperatures (see Fig. 10).

The formation of carbide is apparent from C 1s peak as shown in Fig. 11. This carbon is the dissolved carbon in the alloy which has segregated to the surface at higher temperatures. Its intensity shows a consistent increase with temperature (Fig. 10) and the peak position at 282.4 eV at all temperatures (see Fig. 11) is suggestive of its presence in carbide form, possibly as ZrC/TiC as both Zr and Ti have high reactivity for carbide formation.

Discussion

Room temperature oxidation

The oxygen uptake displayed in Fig. 2 shows two clear different evolution stages: an initial fast increase followed by a slowing down of the oxygen sticking and finally a plateau region. The first stage could be associated with oxide formation via oxygen dissociation and site exchange, and the second one with oxidation via field-assisted migration as suggested in the case of Ti-based alloys [35, 36]. In fact, the slowing down of the oxygen adsorption with increasing exposures may correspond to a slowing down in the oxygen migration capability due to the formation of an initial oxide film.

The oxidation picture that emerges from the results for the single elements presented in section "Results: Room temperature oxidation" suggests that during initial stages of oxidation at room temperature Zr, Be and to some extent Ti get oxidized, while Cu and Ni remain in their elemental forms at/near the oxide–alloy interface. The oxides include species Zr(IV), Be(II), Ti(II)–Ti(IV) possibly in the form of ZrO_2, BeO and several oxides of Ti. The initial oxide film reaches a near constant or saturation coverage at about 300 L. The presence of the metal components in various XPS peaks (Figs. 3–5) and the respective decrease in intensity of the Cu $2p_{3/2}$ and Ni $2p_{3/2}$ peaks upon the initial oxygen exposure up to 1,000 L show that the film is only a few monolayers thick. An estimate based on the escape depth [37, 38] of Ni $2p_{3/2}$ and Cu $2p_{3/2}$ photoelectrons (1.31 and 1.23 nm for Ni $2p_{3/2}$ and Cu $2p_{3/2}$, respectively) and the decrease in their intensity after the formation of saturation coverage layer suggests a thickness of about 0.54 nm for the initial oxide film [36]. In this calculation we assume that Ni and Cu are located just below the oxide layer, in agreement with the depth profiles obtained by Kiene et al. [14] for V4 oxidized in air.

The formation of various oxides can be understood in terms of the known values of the heat of formation for various alloying elements. The heats of formation for BeO, ZrO_2, TiO, Ti_2O_3, NiO and CuO are −1,219.8, −1,101.1, −1,039.8, −1,014.3, −497.7 and −314.8 kJ/mol(O_2), respectively [39]. This suggests that oxides of Be, Zr and Ti (in that order) are likely to be formed first because of their strong affinity for oxygen. Because of the strong reactivity of these elements to oxygen, their segregation to the surface in the presence of oxygen is to be expected. Such segregation may inhibit oxidation of the less reactive alloying elements Cu and Ni that remain at/near the oxide alloy interface in their elemental form. The formation of a continuous oxide film consisting of oxides of Zr, Be and Ti would greatly retard the migration of oxygen through the oxide film. Further, it has been suggested [10] that in the case of the initial oxidation of amorphous Zr–Ni alloys the segregation of Zr to the surface is further facilitated by the smaller size of Zr^{n+} ions (0.109 nm for $n = 1$ and 0.087 nm for $n = 4$) as compared to that of Ni atoms (0.125 nm). This implies that the formation of Zr ions occurs not only at the surface but also at the metal–oxide interface by diffusion of oxygen through the surface oxide layer. The same arguments could be given here also for Zr, Be and Ti oxidation. Of course the migration capability of oxygen through the oxide film is retarded as the film grows thicker and is evident from the appearance of a saturation plateau (Fig. 2). All migrating oxygen atoms are used up in oxidizing highly reactive elements Be, Zr and Ti and it is very likely that no oxygen atoms are available at the metal–oxide interface for a possible oxidation of Cu and Ni.

Oxidation at higher temperatures

The oxidation behaviour at elevated temperatures shows many similarities to the oxidation at room temperature. The biggest changes seem to be induced by the carbon impurity. The following specific changes are deduced from Figs. 7–9:

(i) The Zr, Be and Ti get oxidized at lower temperatures (below 573 K) but at and above 573 K oxides of Zr and Ti get severely reduced (Figs. 7–9). A corresponding reduction in the intensity of O 1s peak at higher temperatures is also noticed (Fig. 10). Possible explanations are a lower sticking coefficient of oxygen on the hot alloy surfaces or a reaction of oxygen with the carbon impurity and desorption of the so-produced gases CO and/or CO_2 into the vacuum. So far we cannot rule out either of these possibilities. Further, it is noteworthy here that these observations pertain to high-temperature oxidation investigated for a fixed dose of 300 L and thus cannot be taken as representative of those at much higher oxygen doses. More measurements at several higher doses are desirable in order to decipher the oxidation mechanism at higher temperatures.

(ii) A small decrease in the intensity of the Be 1s peak (Fig. 9) at higher temperatures is suggestive of a decrease in its enrichment on the surface with increasing temperatures. No dissociation of BeO occurs at these temperatures and it is present on the surface over the entire temperature range (cf. Fig. 9). In fact, the tendency for oxidation of Be increases with increasing temperature as evidenced by increase in the ratio of the intensity of its oxide to metal component peaks (Fig. 9). The smaller size of Be is also favourable for enhancing its segregation to the surface at higher temperatures in presence of oxygen and one would expect to observe an increase in the intensity of the oxide peak of Be with increase in temperature. But, interestingly a decrease in the intensity of the oxide component in the Be 1s spectra is noticed with increase in temperature (Fig. 9). This possibly may arise due to the strong segregation of carbon to the surface and the formation of a carbide layer on the surface (Fig. 11).

(iii) The peak positions for the Ni $2p_{3/2}$ (853.3 eV) and Cu $2p_{3/2}$ (933.1 eV) XPS peaks indicate their presence in metallic forms only during exposures at all temperatures. This behaviour is similar to that observed for these elements at room temperature (see section "Discussion: Room temperature oxidation"). However, it is noteworthy that intensity of Ni $2p_{3/2}$ peaks (see Fig. 12) shows a steady decrease with increasing temperature suggesting that Ni is possibly pushed into the bulk at higher temperatures. After reduction of the major oxides of Zr and Ti on the surface at higher temperatures (573 K and above here) one would have expected an enhancement in the intensity of Ni $2p_{3/2}$ peak due to the decrease in the thickness of the oxide layer.

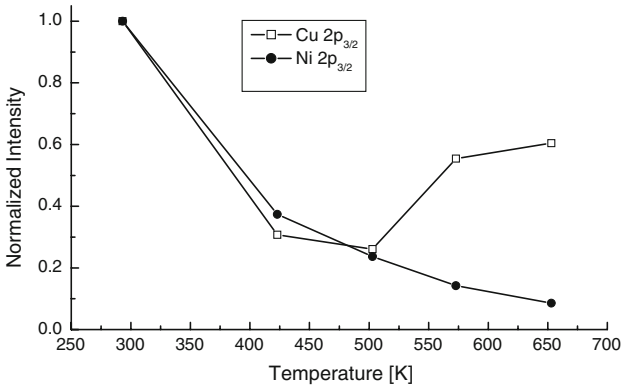

Fig. 12 Normalized XPS intensity ratios for Ni $2p_{3/2}$ and Cu $2p_{3/2}$ peaks versus temperature for in situ oxidation at higher temperatures for a fixed oxygen dose of 300 L

This expected behaviour is indeed observed for the Cu $2p_{3/2}$ peak intensity (see Fig. 12). At first the Cu $2p_{3/2}$ intensity decreases due to the formation of a thicker oxide overlayer on the surface. When the oxide layer thickness is reduced at elevated temperatures, the Cu $2p_{3/2}$ XPS intensity increases again. The intensity changes of copper and nickel for the oxidation at elevated temperatures indicate that copper is only affected by the reduction of oxides at higher temperatures independent of the carbide formation, whereas nickel is pushed into the bulk by both the oxide and the carbide. In view of the approximately similar heat of formation and atomic size values of Ni and Cu, it is difficult to find a possible explanation for this behaviour. In this context it would be worth mentioning that our observations regarding the behaviour of Ni during high-temperature oxidation seem to be consistent with the results reported by Dhawan et al. [18, 23] and Sun et al. [13] on oxidation of other Zr-based bulk alloys, namely $Zr_{65}Cu_{17.5}Ni_{10}Al_{7.5}$ and $Zr_{60}Al_{15}Ni_{25}$, respectively. In both of these investigations it has been suggested that the rate limiting process for high-temperature oxidation of these Zr-based bulk amorphous alloys is the back diffusion of Ni. It is interesting to note here that our observations on Ni and Cu during in situ high-temperature oxidation of $Zr_{46.75}Ti_{8.25}Cu_{7.5}Ni_{10}Be_{27.5}$ are in line with those reported recently by Dhawan et al. [23] on high temperature air oxidation of amorphous $Zr_{65}Cu_{17.5}Ni_{10}Al_{7.5}$. On the basis of the XPS analysis of the air-formed oxide films on amorphous $Zr_{65}Cu_{17.5}Ni_{10}Al_{7.5}$ at high temperatures it was suggested by Dhawan et al. [23] that Cu lies near the oxide–alloy interface while Ni is pushed into the alloy.

(iv) Figure 10 shows the variation of (O 1s/Zr 3d) and (C 1s /Zr 3d) intensity ratios with annealing temperature for specimens exposed to an oxygen dose of 300 L. It is observed from this figure that the (O/Zr) ratio shows an increase up to a temperature of 503 K suggesting the oxidation of Zr, while at higher temperatures there is a drastic

decrease in this ratio indicating the reduction of the oxide. On the other hand the intensity ratio of (C/Zr) shows a slow increase up to 503 K and thereafter a big increase in the ratio is seen suggesting a strong segregation of dissolved carbon impurity from the alloy bulk to the surface. The carbon is present on the surface in carbide form possibly as ZrC/TiC. In fact, similar observations have been made during oxidation of amorphous Zr–Ni alloys and it has been suggested that the formation of these carbides is responsible for the reduction of oxides of Zr and Ti at higher temperatures [11]. The rate controlling process for oxide growth will be the availability of oxygen at the surface vis-a-vis its possible reaction with the carbon impurity segregating to the surface. It would be interesting to note here the fact that carbon impurity in a similar but compositionally different bulk metallic glass has been shown to lead to the formation of an amorphous matrix composite consisting of ZrC particles [40]. However, no attempt was made to investigate these effects induced by segregated carbon in the present study.

In order to confirm the above picture for oxidation at higher temperatures, a zirconium foil and a V4 specimen both with a pre-existing native oxide were gradually heated up to 800 K and during the various stages of heating the XPS peaks of Zr, O and C were recorded (data not shown). The results qualitatively gave the same results. At temperatures of 573 K and above the oxygen intensity decreases and a significant C 1s intensity is present suggesting that dissolved carbon impurity forms a carbide layer at higher temperatures possibly by reduction of pre-existing oxide layer on the surface. It confirms our earlier suggestion that a drastic decrease in the intensity of the oxide components of Zr and Ti (Figs. 7, 8) possibly occurs due to their reduction by the carbon impurity. A simple schematic diagram for the observed oxidation processes occurring on the surface of the bulk amorphous alloy $Zr_{46.75}Ti_{8.25}Cu_{7.5}Ni_{10}Be_{27.5}$ during its in situ high-temperature oxidation for a fixed oxygen dose of 300 L is shown in Fig. 13.

Therefore, the initial oxide film at higher temperatures for a fixed oxygen dose of 300 L consists of oxides of Zr, Be and Ti at temperatures below 573 K while only Be gets oxidized at higher temperatures. Over the entire temperature range, BeO is the most stable one possibly because it exhibits the lowest heat of formation value among all the alloy constituents. At higher temperatures Ni appears to be moved further away from the oxide–alloy interface into the alloy bulk by carbide formation while Cu remains closer to the interface.

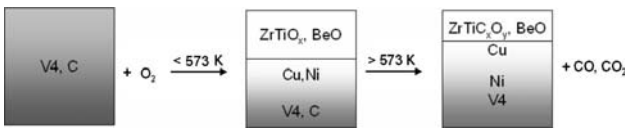

Fig. 13 A schematic diagram for in situ high-temperature oxidation of the bulk amorphous alloy $Zr_{46.75}Ti_{8.25}Cu_{7.5}Ni_{10}Be_{27.5}$ for a fixed oxygen dose of 300 L

Conclusions

XPS investigations of the in situ oxidation of the bulk metallic glass $Zr_{46.75}Ti_{8.25}Cu_{7.5}Ni_{10}Be_{27.5}$ showed that:

(i) the initial oxide film at room temperature consists of oxides of Zr, Be and Ti with major species being Zr(IV) and Be(II), possibly existing as ZrO_2 and BeO while Ni and Cu do not get oxidized. These observations can be understood in terms of the heats of formation for various alloying elements suggesting the preferential oxidation of the reactive elements (Zr, Be and Ti) due to their segregation to the surface in presence of oxygen.

(ii) the initial oxide film formed at higher temperatures for a fixed oxygen dose of 300 L consisted oxides of Zr, Be and Ti (possibly as ZrO_2, BeO and lower valent suboxides of Ti) at temperatures below 573 K, while at higher temperatures oxides of Zr and Ti were reduced by a reaction with the carbon impurity. Annealing of the alloy specimen with a pre-existing native oxide film also showed a decrease in the (O/Zr) intensity ratio at temperatures around 573 K and above suggesting a similar reduction of ZrO_2 on the surface by segregating carbon. No oxidation of Cu and Ni was observed even at these higher temperatures similar to the behaviour observed at room temperature. The intensity of respective XPS peaks for Ni and Cu (Fig. 12) suggests that at higher temperatures Ni is moved beyond the oxide–alloy interface while Cu remains at/near the interface. Also, Be enrichment at the surface is reduced (Fig. 9) due to the strong segregation of the dissolved carbon impurity from the bulk to the surface resulting in the formation of a carbide layer on the surface. This carbide formation also leads to the reduction of oxides at higher temperatures.

Acknowledgement S.K.S. would like to gratefully acknowledge the invitation and the financial support received from the Lehrstuhl für Materialverbunde, Technische Fakultät der Universität Kiel for working as a Visiting Scientist during the course of this work.

References

1. Zhang T, Inoue A, Masumoto T (1991) Mater Trans JIM 32:1505
2. Peker A, Johnson WL (1993) Appl Phys Lett 63:2342. doi: 10.1063/1.110520

3. Hashimoto K (1983) In: Luborsky FE (ed) Amorphous metallic alloys. Butterworths, London, p 471
4. Baiker A, Schlögl R, Armbruster E, Güntherodt H-J (1987) J Catal 107:221. doi:10.1016/0021-9517(87)90287-9
5. Yamashita H, Yoshikawa M, Funabiki T, Yoshida S (1987) J Chem Soc Faraday Trans 83:2883. doi:10.1039/f19878302883
6. Johnson WL (1994) Mater Sci Technol 9:94
7. Sen P, Sarma DD, Budhani RC, Chopra KL, Rao CNR (1984) J Phys F14:565
8. Wang XK, Shen NF, Yang ZS, Gu HC (1995) J Mater Sci Lett 14:1742
9. Asami K, Kimura HM, Hashimoto K, Masumoto T (1995) Mater Trans JIM 36:988
10. WALZ B, Oelhafen P, Güntherodt H-J, Baiker A (1989) Appl Surf Sci 37:337
11. Song Z, Bao X, Wild U, Muhler M, Ertl G (1999) Appl Surf Sci 134:31
12. Schneider S, Sun X, Nicolet M-A, Johnson WL (1995) In: Otooni MA (ed) Science and technology of rapid solidification and processsing. Kluwer Academic Publishers, The Netherlands, p 317
13. Sun X, Schneider S, Geyer U, Johnson WL, Nicolet M-A (1996) J Mater Res 11:2738
14. Kiene M, Strunskus T, Hasse G, Faupel F (1999) Mater Res Soc Symp Proc 554:167
15. Triwikantoro, Toma D, Meuris M, Koester U (1999) J Non-Cryst Solids 250–252:719
16. Köster U, Triwikantoro (2001) Mater Sci Forum 360–362:29
17. Dhawan A, Raetzke K, Faupel F, Sharma SK (2001) Bull Mater Sci 24:101
18. Dhawan A, Raetzke K, Faupel F, Sharma SK (2003) Phys Status Solidi 199:431
19. Sharma SK, Strunskus T, Ladebusch H, Faupel F (2001) Mater Sci Eng A 304–306:747
20. Tam CY, Shek CH (2005) J Mater Res 20:1396
21. Kai W, Hsieh HH, Nieh TG, Kawamura Y (2002) Intermetallics 10:1265
22. Wong CH, Shek CH (2004) Intermetallics 12:1257
23. Dhawan A, Zaporojtchenko V, Faupel F, Sharma SK (2007) J Mater Sci 42:9037. doi:10.1007/s10853-007-1819-z
24. Kai W, Hseih HH, Chen YR, Wang YF, Dang PC (2007) Intermetallics 15:1459
25. Hsieh HH, Kai W, Huang RT, Pan MX, Nieh TG (2004) Intermetallics 12:1089
26. Liu L, Chan KC (2005) Appl Phys A Mater Sci Process 80:1737
27. Ehmler H, Heesemann A, Rätzke K, Faupel F, Geyer U (1998) Phys Rev Lett 80:4919
28. Busch R, Johnson WL (1998) Mater Sci Forum 269–272:577
29. Macht M-P, Wei Q, Wanderka N, Sieber I, Deyneka N (2000) Mater Sci Forum 343–346:173
30. Moulder JF, Stickle WF, Sobol PE, Bomben KD, Chastain J (1992) Handbook of X-ray photoelectron spectroscopy. Perkin-Elmer, Physical Electronics Division, Eden Prairie
31. Nishino Y, Krauss AR, Lin Y, Gruen DM (1996) J Nucl Mater 228:346
32. Kaufmann R, Klewe-Nebenius H, Moers H, Pfennig G, Jennet H, Ache HJ (1988) Surf Interface Anal 11:502
33. Zaporozchenko V, Stepanova MG (1995) Prog Surf Sci 49:155
34. Satoh H, Nakane H, Adachi H (1996) Appl Surf Sci 94–95:247
35. Lee PA, Stork KE, Maschoff BL, Nebesny KW, Armstrong NR (1991) Surf Interface Anal 17:48
36. Vaquila I, Passeggi MCG Jr, Ferron J (1996) Appl Surf Sci 93:247
37. Seah MP, Dench WA (1979) Surf Interface Anal 1:2
38. Ertl G, Küppers J (1985) Low energy electron and surface chemistry. VCH, Weinheim, p 78
39. Lide DR (ed) (1991–1992) CRC handbook of chemistry and physics, 72nd edn. CRC Press, Boca Raton
40. Wang WH, Bian PW, Zhang Y, Pan MX, Zhao DQ (2002) Intermetallics 10:1249